SeaWiFS-derived products in the Baltic Sea: performance analysis of a simple atmospheric correction algorithm

OCEANOLOGIA, 45 (4), 2003.
pp. 655–677.

KEYWORDS
Baltic Sea
Remote sensing
SeaWiFS
Atmospheric correction
Ocean colour
Radiative transfer

Barbara Bulgarelli
Frédéric Mélin
Giuseppe Zibordi

Joint Research Centre of the European Commission,
Institute for Environment and Sustainability,
Inland and Marine Waters Unit,
TP272; IT–21020 Ispra (VA), Italy;

e-mail: barbara.bulgarelli@jrc.it

Manuscript received 28 August 2003, reviewed 13 October 2003, accepted 29 October 2003.

Abstract

The accuracy analysis of an approximate atmospheric correction algorithm for the processing of SeaWiFS data has been investigated for the Baltic Sea. The analysis made use of theoretical radiances produced with the FEM radiative transfer code for representative atmosphere-water test cases. The study showed uncertainties in the determination of the aerosol optical thickness at 865 nm and of the Ångström exponent lower than ±5% and ±10%, respectively. These results were confirmed by the analysis of 59 match-ups between satellite-derived and *in situ* measurements for a site located in the central Baltic. Because of the relatively high yellow substance absorption, often combined with the slanted solar illumination, the retrieval of the water-leaving radiance in the blue part of the spectrum appeared to be highly degraded, to the extent that almost no correlation was found between retrieved and simulated values. Better results were obtained at the other wavelengths. The accuracy in the estimation of the remote sensing reflectance ratio R_{35} decreased with diminishing chlorophyll *a* concentration and increasing yellow substance absorption, ranging between ±7% and ±47%.

The propagation of R_{35} uncertainties on chlorophyll a estimation was quantified. Keeping the same atmosphere-water conditions, the atmospheric correction scheme appeared sensitive to seasonal changes in the Sun zenith.

1. Introduction

The Baltic Sea is a semi-enclosed basin with specific hydrological and biochemical traits, as well as a marine area significantly affected by human activities (Larsson et al. 1985). More specifically, biological cycles show a diverse spatio-temporal distribution and species succession (e.g. Witek et al. 1997, Zernova 1997, Siegel et al. 1999, Neumann et al. 2002), with strong spring algal blooms, characterized by complicated patterns, and low biological activity in winter. Summer usually brings the conspicuous appearance of cyanobacteria blooms (Larsson et al. 2001), which can result in the surface accumulation of filamentous formations, readily detected from space (Kononen & Leppänen 1997, Siegel & Gerth 1999). More generally, Baltic waters display a large variability in their inherent and apparent optical properties (e.g. Olszewski et al. 1992, Kowalczuk 1999, Darecki et al. 2003). Two optical characteristics are particular features of the Baltic area. Firstly, the levels of absorption by coloured dissolved organic matter (yellow substance) are quite high, and account for a large part of the total absorption of the water, particularly in the blue region of the spectrum (Ferrari et al. 1996, Kowalczuk & Darecki 1998). Secondly, the geographic position of the Baltic Sea, whose lowest latitude is around 54°, implies a strong seasonal cycle in surface insolation, and considerably slanted solar illuminations (the solar zenith angle is never lower than about 30°).

While the first arguments underline the need for long-term synoptic observations of the marine ecosystem, which only remote sensing can provide, the latter arguments point out the difficulties encountered in the processing of remotely sensed data for the Baltic area. Indeed, high solar zenith angles enhance atmospheric multiple scattering, while strong yellow substance absorptions decrease the water signal. Both aspects, even more so when concurrent, render the accurate performance of an atmospheric correction code a challenging task.

A processing tool has been developed (Bulgarelli & Mélin 2000, Mélin et al. 2002) for the analysis of data from the Sea-viewing Wide-Field-of-view Sensor (SeaWiFS, Hooker & Esaias 1993), a visible to near-infrared multispectral scanner that has been providing global coverage of the oceans since 1997.

The processing tool makes use of a simple atmospheric correction method (Sturm & Zibordi 2002) which accounts for Rayleigh multiple scattering, aerosol single scattering and Rayleigh-aerosol coupling. The

optical contribution of the water surface for the near infrared (NIR) channels is accounted for iteratively by a so-called turbid water correction (Mélin et al. 2003). Integral to the atmospheric correction scheme is the vicarious calibration procedure, which, by making use of *in situ* marine and atmospheric data, minimizes the model inaccuracy and sensor absolute calibration uncertainty (Sturm & Zibordi 2002, Ohde et al. 2002). The accuracy of the derived products has been extensively assessed for mid-latitude European regions, and more specifically for the northern Adriatic Sea (Bulgarelli & Zibordi 2003, Mélin et al. 2003). This paper aims at extending the analysis to the Baltic Sea.

By using simulated top-of-atmosphere (TOA) radiance data, the accuracy of the atmospheric correction method in the retrieval of (i) aerosol optical thickness, (ii) water-leaving radiance, and (iii) remote sensing reflectance ratios is evaluated at the SeaWiFS channels for atmospheric and water parameters typical of the Baltic Sea. This assessment is supported by the comparison of actual SeaWiFS-derived aerosol products with field measurements of the area.

2. Material and methods

2.1. Background

A detailed description of the data processing scheme and the included atmospheric correction algorithm are given in Sturm & Zibordi (2002), Bulgarelli & Zibordi (2003) and Mélin et al. (2003). For completeness, the main conclusions of the accuracy assessment for the northern Adriatic Sea are recalled here.

By using simulated TOA radiance data, an accuracy analysis of the atmospheric correction method in the estimation of aerosol optical thickness τ_a, water-leaving radiance L_w, and remote sensing reflectance ratios was performed for atmospheric and water parameters typical of mid-latitude European regions, with specific reference to the northern Adriatic Sea. The analysis (Bulgarelli & Zibordi 2003) indicated that the aerosol optical thickness at 865 nm and the aerosol Ångström exponent can be estimated with uncertainties lower than $\pm 5\%$ and $\pm 8\%$, respectively. It also demonstrated an increase of uncertainties in the estimation of the water-leaving radiance with decreasing pigment concentration and increasing yellow substance absorption. Finally, it showed uncertainties of $\pm 10\%$ in the estimation of the remote sensing reflectance ratio between the 490 and 555 nm SeaWiFS channels.

For the same region, an extensive validation of SeaWiFS-derived products, including aerosol optical thickness, water-leaving radiance, chlorophyll *a* concentration (Chl), total suspended matter concentration (TSM), and diffuse attenuation coefficient K_d, was performed with *in situ* data collected in the northern Adriatic Sea for the period September 1997 – May 2002 (Zibordi et al. 2002, Mélin et al. 2003). The results exhibited mean relative differences between *in situ* and satellite-derived aerosol optical thicknesses less than 23% in the spectral range 443 to 865 nm, whereas the mean relative difference for the remote sensing reflectance ratio at 490 and 555 nm was found equal to 8%. By applying regional empirical bio-optical algorithms for Chl, TSM, and K_d at 490 nm, the analysis of coincident, *in situ* and satellite-derived values showed respective mean relative differences of 40%, 28% and 30% .

The two analyses supported each other: the differences in the results are justified by additional sources of uncertainties affecting the complete processing chain for SeaWiFS data, the *in situ* measurements, and the variability inherent to the comparison of pixel-size satellite values with point measurements.

2.2. Elements of the simulation scheme

The highly accurate FEM radiative transfer code, whose description and accuracy are given in Bulgarelli et al. (1999), is used to simulate the radiance contributions at the sensor. The simulations are performed at SeaWiFS centre-wavelengths ($\lambda_1 = 412$, $\lambda_2 = 443$, $\lambda_3 = 490$, $\lambda_4 = 510$, $\lambda_5 = 555$, $\lambda_6 = 670$, $\lambda_7 = 765$, $\lambda_8 = 865$ nm) for a coupled atmosphere-ocean system with a flat sea surface and in the absence of whitecaps (assumptions reasonable for wind speeds lower than about 4 m s^{-1}), using the same atmosphere-water model described in Bulgarelli & Zibordi (2003). For simplicity the TOA solar irradiance is assumed equal to unity.

Several combinations of geometric, atmospheric and marine parameters have been chosen (see Table 1) as representative of the Baltic Sea. Each combination defines a test case.

The viewing angle θ_v of the space sensor is only considered in the range 20°–50°, as it is restricted by the SeaWiFS tilt angle and scan edge. The relative azimuth $\Delta\phi$ between the sensor and the Sun, is taken in the range 0°–70°, as defined by the SeaWiFS observation geometry for the region. The solar zenith angle θ_0 is chosen to vary between 30° and 65°. The lower limit for θ_0 is imposed by the geographic position of the Baltic Sea, where the southernmost latitude is around 54°N.

The maritime and continental aerosol single scattering albedo ω_{0a} (IAMAPRC 1984) are selected as typical cases. The range of variability

Table 1. Geometric, atmospheric and marine parameters used in the simulations. The parameters defining the standard case are given in bold, while the parameters defining the other cases are given in brackets

Satellite zenith angle	θ_v	**20°–30°–40°–50°**
Relative azimuth between the planes of illumination and observation	$\Delta\phi$	**0°–40°–70°**
Sun zenith angle	θ_0	**45°** (30°–50°–65°)
Ångström exponent	ν	**1.4** (1.0–1.8)
Ångström coefficient	α	**0.05** (0.02–0.08)
Aerosol single scattering albedo	ω_{0a}	**Maritime***, **Continental***
Chlorophyll a concentration	Chl [mg m^{-3}]	**0.3–3.0–10.0**
Yellow substance absorption coefficient at 440 nm	$a_{ys}(440)$ [m^{-1}]	**0.1443–0.4137–0.6831**
Spectral slope of exponential decay of the yellow substance absorption coefficient	S_{ys} [nm^{-1}]	**0.0193** (0.0145–0.0240)

* according to WMO (IAMAPRC 1984).

for the Ångström coefficient α and exponent ν is chosen to represent clear atmospheres in the Baltic Sea. The case with α equal to 0.02 corresponds to a very clear atmosphere. The middle and high values of α are associated with $\tau_a(550)$ of 0.09 and 0.23, respectively. Out of an extensive literature review, Smirnov et al. (2002) listed values of $\tau_a(550)$ in the range of 0.11–0.28. At a measurement site in the central Baltic (Gotland Island, see below) climatological mean values of 0.06 and 1.4 have been observed for α and ν, respectively. In the southern Baltic, Kuśmierczyk-Michulec et al. (2001) found median values of 0.17 and 0.14 for $\tau_a(555)$ in July 1997 and March 1998, respectively, and a large variability in the Ångström exponent (0.3–1.7). Higher values of $\tau_a(555)$ may be regularly measured in coastal areas (0.10–0.50, Kuśmierczyk-Michulec & Marks 2000).

The chlorophyll a concentrations Chl are selected to represent diverse conditions. Similarly, different absorption coefficients of yellow substance $a_{ys}(\lambda)$ and associated slope coefficients S_{ys} of exponential decay are chosen to represent the minimum, mean and maximum experimental conditions observed in the Baltic Sea. Schwarz et al. (2002) indicate a mean $a_{ys}(440) = 0.4137$ m^{-1}, with standard deviation $\sigma_a = 0.2694$ m^{-1}, and a mean slope coefficient $S_{ys} = 0.0193$ nm^{-1}, with a narrow standard deviation $\sigma_s = 0.0024$ nm^{-1}. Kowalczuk (1999) observed that yellow substance absorption in the southern Baltic Sea is characterized by significant seasonal variations (with a maximum in spring, and a minimum in autumn-winter,

in relation to the biological cycle and to the hydrological pattern of riverine discharge and vertical mixing of the water column) and significant spatial variations (the highest values of yellow substance absorption coefficient are in bay water and the lowest in open-sea water in all seasons; the coastal zone shows intermediate values). Conversely, Kowalczuk (1999) observed that the coefficient S_{ys} is subject to minor seasonal and spatial variations, which suggests that the average composition of humic substances in the southern Baltic remains stable, and that fulvic acids are the dominant fraction of coloured dissolved organic matter. A general tendency for higher absorption values to be associated with lower slopes is commonly observed (Kowalczuk 1999, Højerslev & Aas 2001, Schwarz et al. 2002).

2.3. Accuracy assessment of the atmospheric correction method

The analysis is carried out assuming that the radiance at the sensor is not affected by noise and that the water-leaving radiance in the NIR is known exactly and, for simplicity, assumed negligible. The influence of incorrect predictions of the NIR water-leaving radiance on the overall accuracy of the atmospheric correction algorithm has been already discussed in Bulgarelli & Zibordi (2003).

The atmospheric correction scheme ingests as input data (i) the sensor viewing geometry, (ii) the Sun zenith and azimuth, (iii) the simulated TOA total, $L_{tot}(\lambda_i)$, and Rayleigh, $L_R(\lambda_i)$, radiances at each λ_i, and produces (i) the aerosol optical thickness at λ_8, $\tau_a(\lambda_8)$, (ii) the aerosol Ångström exponent ν, (iii) the water-leaving radiance $L_w(\lambda_i)$ at $\lambda_1 - \lambda_6$, and (iv) derived products such as the remote sensing reflectance ratios $R_{ij} = R_{rs}(\lambda_i)/R_{rs}(\lambda_j)$, where $R_{rs}(\lambda) = L_w(\lambda)/E_d(\lambda)$ (with $E_d(\lambda)$ the downwelling irradiance above the sea surface).

The accuracy analysis is based on (i) the relative percentage uncertainty ε of the estimated X_e versus simulated X_s quantities, computed for each test case according to

$$\varepsilon(X) = \frac{X_e - X_s}{X_s} \times 100, \tag{1}$$

and on (ii) the mean $< \varepsilon >$ and the standard deviation σ_ε relative to the Gaussian fit of the ε distribution. In order to support the accuracy analysis of data that do not follow a Gaussian distribution, the percentage root mean square relative difference *RMSrd* is introduced, and defined as

$$RMSrd(X) = \sqrt{\frac{1}{N}\sum_{k=1}^{N}\left[\frac{X_e - X_s}{X_s}\right]^2} \times 100, \tag{2}$$

where N represents the number of selected test cases.

2.4. Vicarious calibration procedure

The vicarious calibration procedure is performed to optimize the code for the selected region, in a way similar to the method followed for operational codes (Eplee et al. 2001, Sturm & Zibordi 2002).

At first, the vicarious calibration coefficient V_{cf} at λ_8 is computed estimating the total radiance at the sensor from exact values of $\tau_a(\lambda_8)$. Afterwards, an analogous procedure is used to compute the V_{cf} at λ_7. Fig. 1a shows the scatter plots of estimated versus simulated $L_{tot}(\lambda_{7,8})$ for

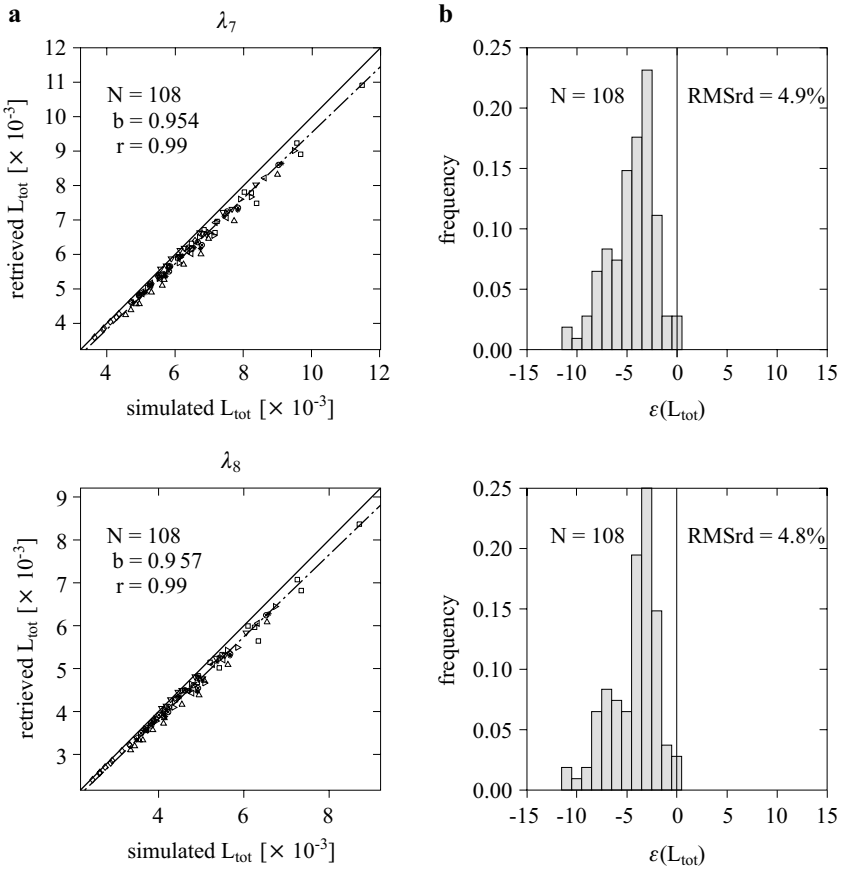

Fig. 1. Plots of retrieved $L_{tot}(\lambda_{7,8})$ versus simulated $L_{tot}(\lambda_{7,8})$ (a) and frequency histograms of $\varepsilon(L_{tot})$ (b). Data are for all atmospheric test cases, assuming a TOA solar irradiance equal to unity. Each point represents a test case. Circle: standard cases; diamond: $\alpha = 0.02$; square: $\alpha = 0.08$; leftward triangle: $\nu = 1.0$; rightward triangle: $\nu = 1.8$; downward triangle: $\theta_0 = 30°$; star: $\theta_0 = 50°$; upward triangle: $\theta_0 = 65°$; x-sign: continental aerosol single scattering albedo. The dashed-dotted line is the linear regression line of slope b, r its correlation coefficient. *RMSrd* is the root mean square of relative differences

all atmospheric test cases, and Fig. 1b displays the frequency histogram of $\varepsilon(L_{tot})$. Estimated and simulated quantities display a clear linear relationship. The dotted-dashed line represents the linear regression of data, whose slope b is adopted as vicarious calibration coefficient (specifically, $b = 0.954$ at λ_7 and $b = 0.957$ at λ_8).

Subsequently, the computation of the V_{cf} at $\lambda_1 - \lambda_6$, is performed by estimating the total radiance at the sensor from exact water-leaving radiance L_w at each λ_i. For the different centre-wavelengths, the regression slopes of estimated $L_{tot}(\lambda_i)$ as a function of simulated $L_{tot}(\lambda_i)$ range between 0.954 and 0.971, while the coefficients of correlation r are always larger than 0.998.

3. Results

3.1. Accuracy of the estimated atmospheric parameters

Fig. 2a shows the scatter plot of retrieved versus simulated $\tau_a(\lambda_8)$. The linear regression line, whose slope b is used to describe the average difference between retrieved and true (i.e. simulated) values, is indistinguishable from the 1:1 line. The frequency histogram of $\varepsilon(\tau_a(\lambda_8))$ and its Gaussian fit are displayed on Fig. 2b. The Gaussian mean $< \varepsilon >$ and standard deviation σ_ε suggest that $\tau_a(\lambda_8)$ is retrieved with an average uncertainty of $\pm 5\%$ for 68% of the cases.

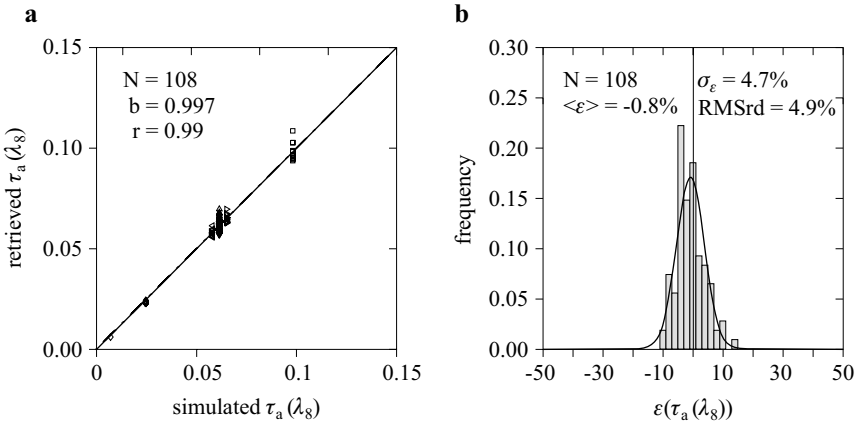

Fig. 2. Plots of retrieved versus simulated $\tau_a(\lambda_8)$ (a) and frequency histogram of $\varepsilon(\tau_a(\lambda_8))$ and its Gaussian fit (b). Each point represents a test case (see Fig. 1). The dashed-dotted line is the linear regression line of slope b, r its correlation coefficient. $< \varepsilon >$ and σ_ε are the mean and standard deviation of the Gaussian fit, respectively. *RMSrd* is the root mean square of relative differences

Similarly, Fig. 3 shows the scatter plot of retrieved versus simulated ν, as well as the frequency histogram of $\varepsilon(\nu)$ and its Gaussian fit. The Gaussian mean $< \varepsilon >$ and standard deviation σ_ε indicate that ν is retrieved with an average uncertainty of $\pm 10\%$ for 68% of the cases.

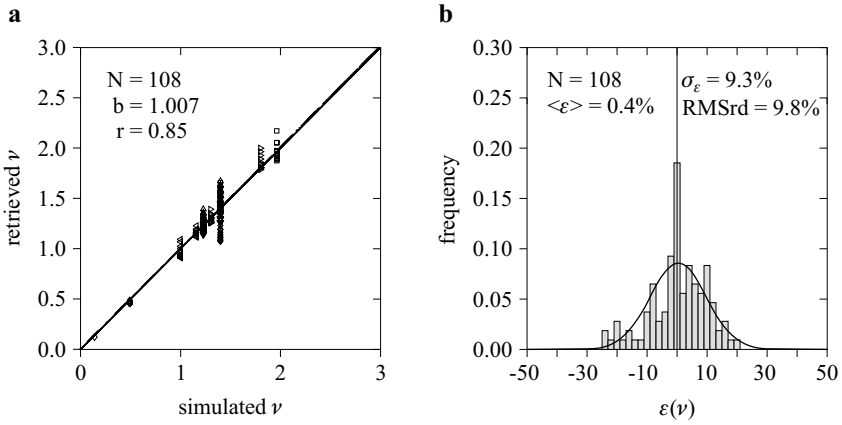

Fig. 3. Plots of retrieved versus simulated ν (a) and frequency histogram of $\varepsilon(\nu)$ and its Gaussian fit (b). Each point represents a test case (see Fig. 1). The dashed-dotted line is the linear regression line of slope b, r its determination coefficient. $< \varepsilon >$ and σ_ε are the mean and standard deviation of the Gaussian fit, respectively. *RMSrd* is the root mean square of relative differences

These results are in close agreement with those determined for mid-latitude European regions.

3.2. Accuracy of the estimated water-leaving radiance

Figs 4.1a and 4.2a illustrate the accuracy in retrieving the water-leaving radiance L_w, at representative centre-wavelengths λ_1, λ_3, λ_5 and λ_6, through the plots of estimated versus simulated L_w for all test cases characterized by a mean yellow substance absorption ($a_{ys}(440) = 0.4137$ m^{-1}, $S_{ys} = 0.0193$ nm^{-1}). At each centre-wavelength, Figs 4.1b and 4.2b show the frequency histograms of the percentage relative uncertainty $\varepsilon(L_w)$ and their Gaussian fits, for the different Chl values.

As a result of the vicarious calibration procedure, the linear regression slopes are very close to 1 at each centre-wavelength. If the V_{cf} values obtained for mid-latitude European regions were adopted in alternative to those produced in this study, a bias (particularly relevant in the blue channels) would characterize the intercomparison results.

The scattering on ε, identified by the Gaussian standard deviation σ_ε, is extremely high at λ_1 and at λ_2 (not shown here). Two phenomena

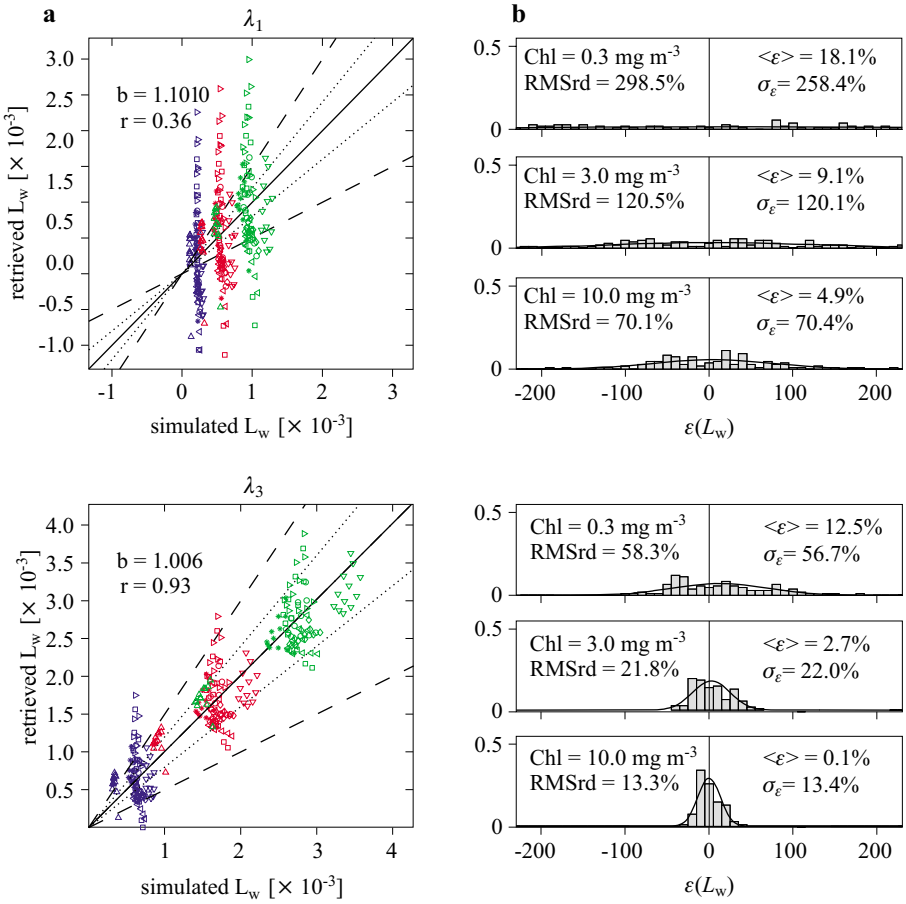

Fig. 4.1. Plots of retrieved versus simulated L_w (the TOA solar irradiance is assumed equal to unity) (a) and frequency histograms, with Gaussian fit, of $\varepsilon(L_w)$ for each selected chlorophyll a concentration Chl (b). Data are for centre-wavelengths λ_1 and λ_3, and for all test cases characterized by a mean yellow substance absorption ($a_{ys}(440) = 0.4137$ m^{-1}, $S_{ys} = 0.0193$ nm^{-1}). Each point represents a test case (see Fig. 1). Blue marks are for Chl = 0.3 mg m^{-3}, red marks for Chl = 3.0 mg m^{-3}, green marks for Chl = 10.0 mg m^{-3}. The dashed-dotted line is the linear regression line of slope b. The dotted and dashed lines delimit the $|\varepsilon(L_w)| < 20\%$ and $|\varepsilon(L_w)| < 50\%$ regions, respectively; r is the correlation coefficient. $< \varepsilon >$ and σ_ε are the mean and standard deviation of the Gaussian fit, respectively. *RMSrd* is the root mean square of relative differences

sum up at these wavelengths: (i) the water signal is lowered by the high yellow substance absorption, and (ii) significant uncertainties in the estimate of the atmospheric radiance occur due to misestimated multiple scattering contributions. The previous study performed for mid-latitude European regions already pointed out that uncertainties in the water-leaving

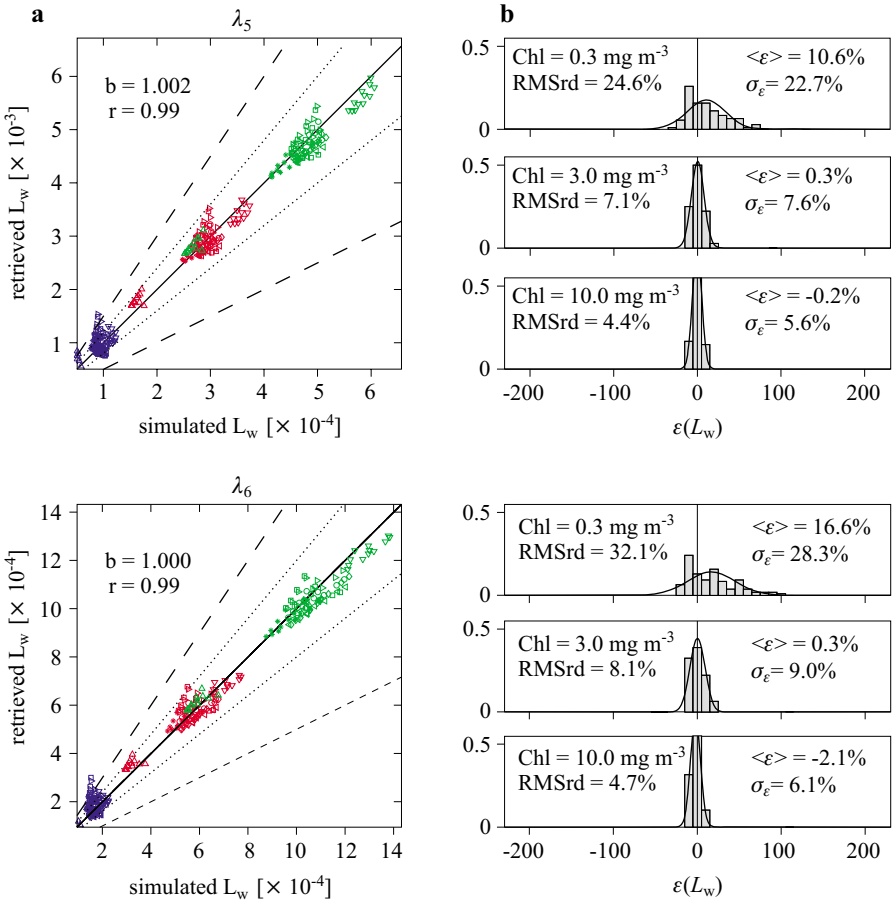

Fig. 4.2. As in Fig. 4.1 but for centre-wavelengths λ_5 and λ_6. Note the different scales for the axis

radiance increase with increasing yellow substance absorption. As expected, the high yellow substance concentrations characterizing the Baltic Sea exacerbate the phenomenon, so that almost no correlation is found between simulated and retrieved water-leaving radiance at λ_1, particularly for low Chl values.

More accurate results are obtained at $\lambda > \lambda_2$, particularly for cases characterized by low atmospheric multiple scattering and high Chl concentration.

3.3. Accuracy in the computation of derived products

Various bio-optical algorithms for chlorophyll *a* estimation make use of the ratio R_{35} between the remote-sensing reflectances at λ_3 and λ_5. Fig. 5 shows the frequency histograms of the percentage relative uncertainty of the

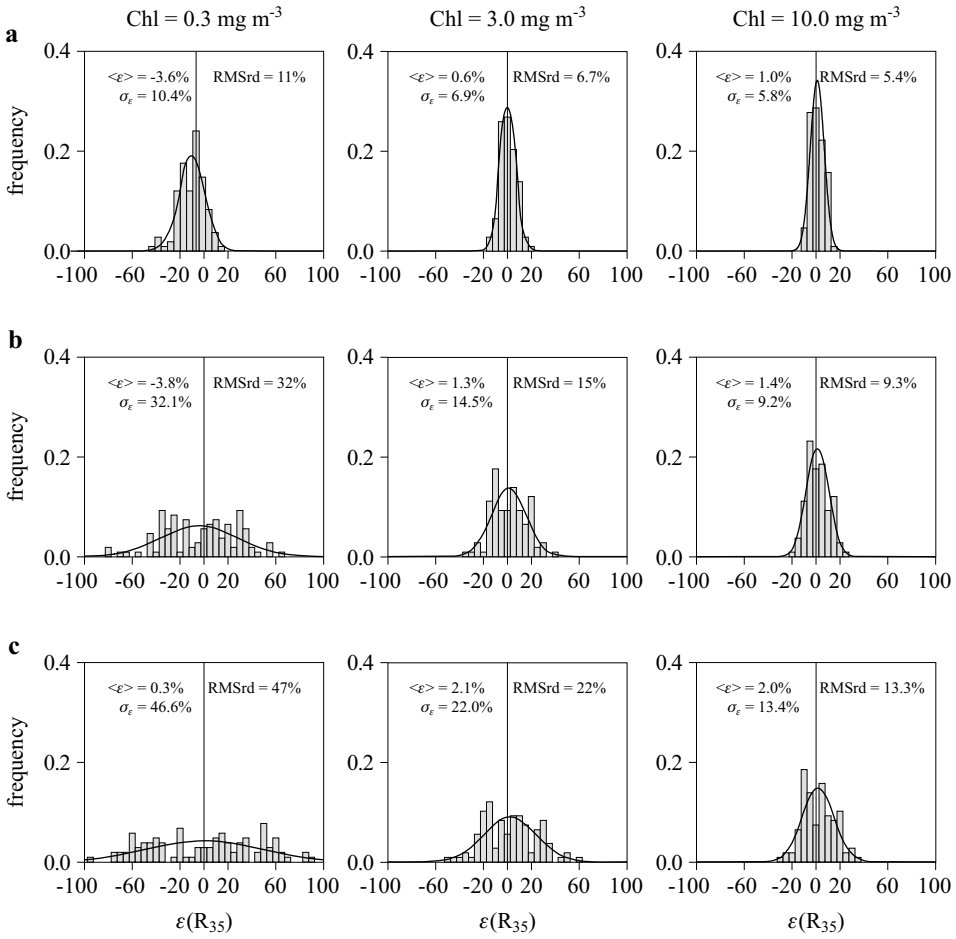

Fig. 5. Frequency histograms, with Gaussian fits, of $\varepsilon(R_{35})$ for each selected chlorophyll a concentration Chl and for minimum (a), mean (b) and maximum (c) yellow substance absorption coefficient $a_{ys}(440)$ ($S_{ys} = 0.0193\ \mathrm{nm}^{-1}$)

reflectance ratio, $\varepsilon(R_{35})$, and the related Gaussian fits, for different chlorophyll a concentrations and yellow substance absorptions ($a_{ys}(440) = 0.1443$, 0.4137, $0.6831\ \mathrm{m}^{-1}$, $S_{ys} = 0.0193\ \mathrm{nm}^{-1}$). The Gaussian means $< \varepsilon >$ indicate the tendency to underestimate R_{35} for low Chl values (about -4%), and to slightly overestimate R_{35} for high Chl values ($+1$–2%). The scattering on ε, identified by the Gaussian standard deviation σ_ε, ranges between 6% and 47%, strongly increasing with Chl decrease and $a_{ys}(440)$ increase. For low Chl associated with medium-high $a_{ys}(440)$, the retrieval of R_{35} is highly degraded.

Minute differences in the results are obtained when varying S_{ys} in its assumed range of variation. Nevertheless, it is possible to observe that σ_ε

increases when S_{ys} decreases: the absorption coefficient of yellow substance at λ_3 and λ_5 is higher for lower values of S_{ys}. A broader range of variation for S_{ys} suggested in various studies (Kowalczuk 1999, Højerslev & Aas 2001) and particularly the high absorption values associated with relatively low spectral slopes (Kowalczuk 1999, Højerslev & Aas 2001, Schwarz et al. 2002) would exacerbate these findings.

Clearly, in the estimation of Chl from remote sensing reflectance ratios, two sources of error add up: the uncertainties affecting the remote sensing reflectance ratio itself and the inaccuracies introduced by the bio-optical algorithm. It is not the aim of this work to assess the accuracy of bio-optical algorithms. Hence, hereafter only the effects of propagation of the

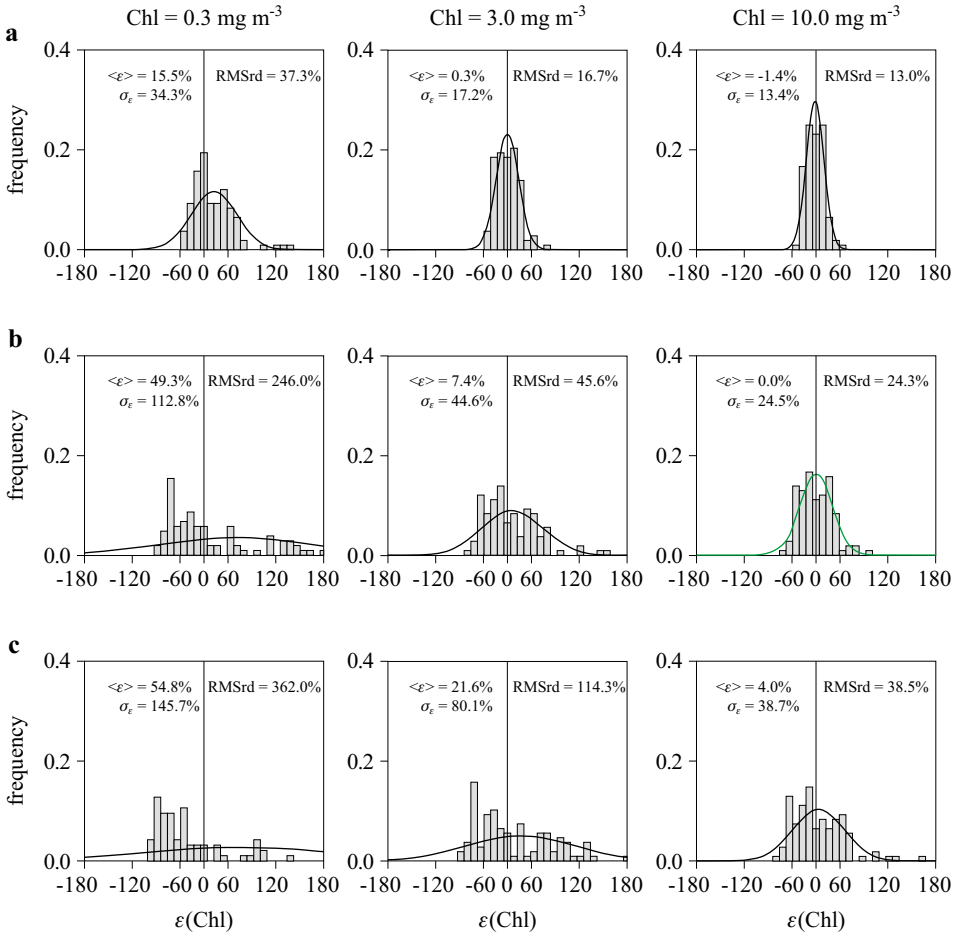

Fig. 6. Frequency histograms, with Gaussian fits, of ε(Chl) for each selected chlorophyll *a* concentration Chl and for minimum (a), mean (b) and maximum (c) yellow substance absorption coefficient $a_{ys}(440)$ ($S_{ys} = 0.0193\ \mathrm{nm}^{-1}$)

R_{35} uncertainties on Chl estimation will be investigated. For the sake of discussion, the OC2v2 algorithm (Maritorena & O'Reilly 2000), relating Chl and R_{35} values, has been adopted as representative of a band-ratio empirical algorithm. Fig. 6 shows the frequency histogram of ε(Chl), i.e. the relative percentage difference between Chl values obtained using retrieved and simulated R_{35} values into the OC2v2 algorithm. In agreement with the conclusions drawn for the retrieval of R_{35}, the estimate of Chl is degraded for low concentrations associated with high yellow substance absorption. As a whole, σ_ε(Chl) is amplified threefold with respect to $\sigma_\varepsilon(R_{35})$, whereas *RMSrd* may be increased even more.

3.4. Uncertainties induced by seasonal variation of the solar zenith angle

As already observed by Bulgarelli & Zibordi (2003), the seasonal variation of the Sun's position may induce seasonal variations in the method's accuracy. Case studies have been investigated for the Island of Gotland, a site located in the central Baltic (lat. 57°55′N, long. 18°56′E), and a component of the AErosol RObotic NETwork (AERONET, Holben et al. 1998). The case studies have been defined for a SeaWiFS overpass at about 12:00 GMT, Sun zenith angle ranging between 37° and 83° over the year, an average viewing geometry given by $\theta_v = 25°$ and $\Delta\phi = 30°$, the standard atmospheric conditions listed in Table 1, a mean yellow substance absorption (i.e. $a_{ys}(440)$=0.4137 m^{-1}, S_{ys}=0.0193 nm^{-1}) and all three chlorophyll a concentrations (i.e. Chl = 0.3, 3.0, 10.0 mg m^{-3}).

Under the selected conditions, the atmospheric correction code gave raise to extremely large errors for θ_0 around 80° (December and January; no

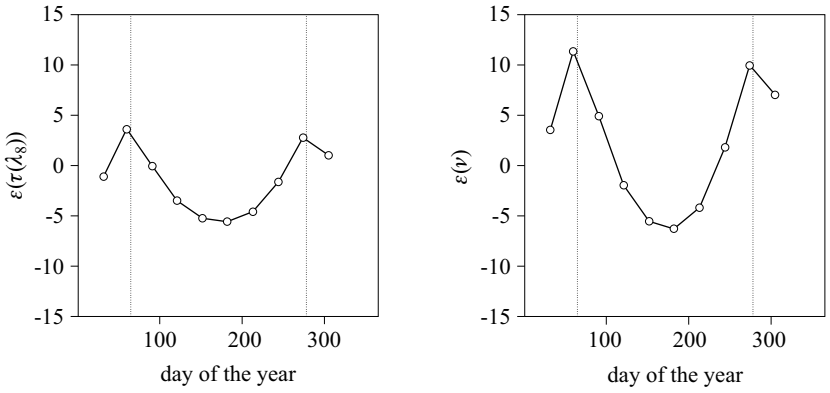

Fig. 7. Seasonal variation of $\varepsilon(\tau_a(\lambda_8))$ and $\varepsilon(\nu)$ for a standard atmosphere and for a SeaWiFS overpass at about 12:00 GMT over the Baltic Sea (lat. 57°55′N, long. 18°56′E). The dotted lines delimit a region for which $\theta_0 < 65°$

operational ocean colour imagery covering the Baltic is actually provided for those months). The results obtained for the rest of the year are hereafter presented.

The seasonal variation of $\varepsilon(\tau_a(\lambda_8))$ and $\varepsilon(\nu)$ as a function of the day of the year are presented in Fig. 7. Both plots show an overestimate for winter (i.e. high θ_0) and an underestimate for summer (i.e. low θ_0). The seasonal variation of $\varepsilon(\tau(\lambda_8))$ and $\varepsilon(\nu)$ is in the range $\pm 5\%$ and $(-7\%, +12\%)$, respectively. The uncertainty fall-off for $\theta_0 < 65^\circ$ is probably due to uncertainty compensations within the correction scheme.

The seasonal variation of $\varepsilon(L_w)$ for λ_1, λ_3, λ_5 and λ_6, and for different Chl values is shown in Fig. 8. The $\varepsilon(L_w)$ range of variation increases on Chl decrease and reaches its maximum at λ_1. In addition, the inversion

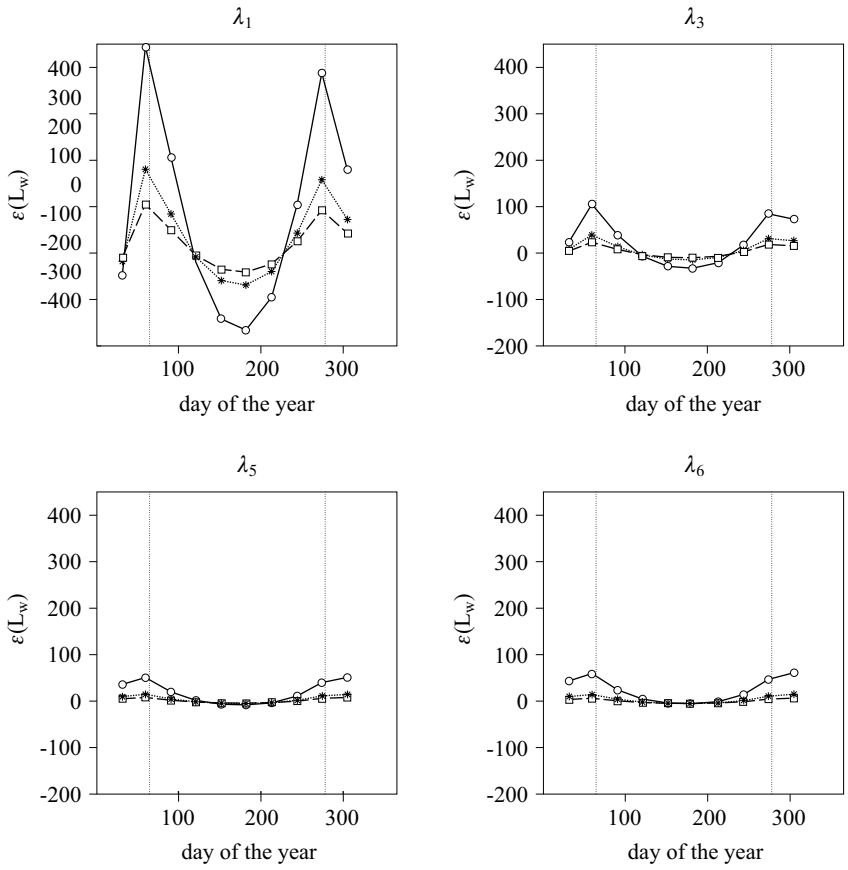

Fig. 8. Seasonal variation of $\varepsilon(L_w)$ for mean yellow substance absorption and ($\circ$) Chl = 0.3 mg m^{-3}, ($*$) Chl = 3.0 mg m^{-3}, ($\square$) Chl = 10.0 mg m^{-3}. Data were produced under the same conditions of Fig. 7 and for centre-wavelengths λ_1, λ_3, λ_5, λ_6

scheme tends to overestimate the water-leaving radiance in winter and to underestimate it in summer.

Fig. 9 shows the seasonal variations of $\varepsilon(R_{35})$ and ε(Chl) for the different input Chl values. $\varepsilon(R_{35})$ is negative in summer and positive in winter, while ε(Chl) has an opposite trend. The range of variation of $\varepsilon(R_{35})$ is within $\pm 40\%$ and strongly increases on Chl decrease. Likewise, the range of variation of ε(Chl) is $\pm 50\%$ for medium-high concentrations, but can reach up to $+100\%$ in summer for low concentrations.

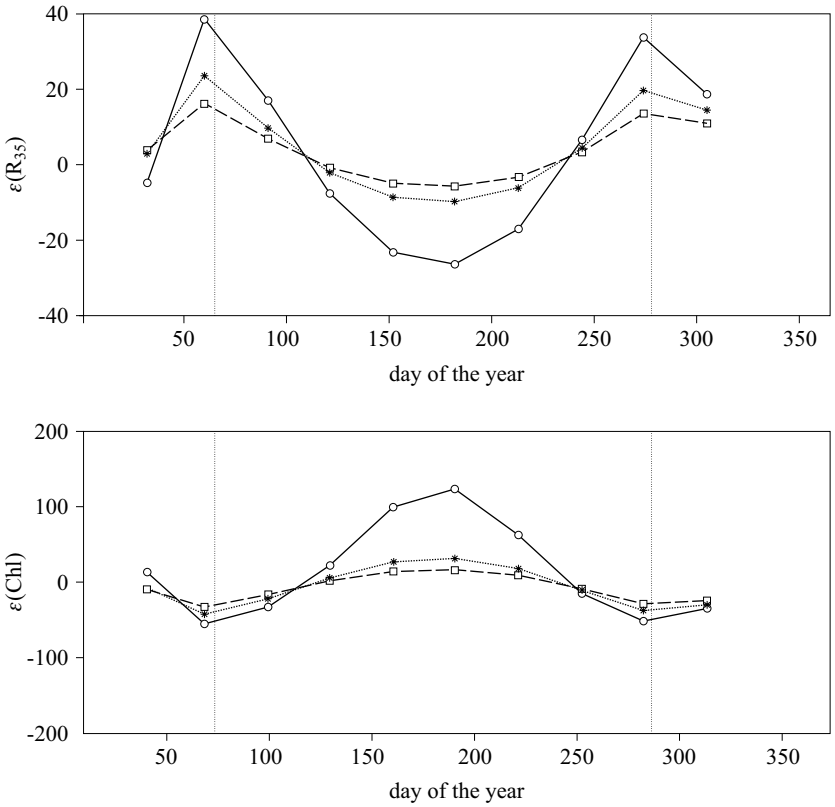

Fig. 9. Seasonal variation of $\varepsilon(R_{35})$ and ε(Chl) for mean yellow substance absorption and ($\circ$) Chl = 0.3 mg m^{-3}, ($*$) Chl = 3.0 mg m^{-3}, ($\square$) Chl = 10.0 mg m^{-3}. Data were produced under the same conditions as in Fig. 7

3.5. Comparison with field measurements

SeaWiFS product validation for the Baltic Sea is here restricted to the aerosol products, making use of *in situ* data collected on Gotland (central Baltic).

The validation was carried out through the analysis of coincident surface optical measurements by the Sun photometer at the site and SeaWiFS overpasses (hereafter called match-ups) for the period 2000–2003. The protocol for the match-up selection implemented in Mélin et al. (2003) for a small oceanographic platform in the northern Adriatic Sea could not be applied here. In fact for Gotland, the pixels closest to the measurement site are land pixels and cannot be included in the comparison analysis. Thus, a large 21x21-pixel square centred on the measurement site is first isolated. Then, in that area, assumed representative of the local atmosphere, the cloud-free marine 5x5-pixel square closest to the site is searched and used for the comparison. A match-up is considered valid if it fulfils the following conditions: (i) at least 3 field measurements sequences are available within ± 1 hour of the satellite overpass; (ii) the satellite and Sun zenith angles are lower than 56° and 70°, respectively; (iii) the atmospheric correction gives valid results on all 25 pixels for the aerosol optical thickness $\tau_a(\lambda)$ in all 8 channels, and for the normalized water-leaving radiance (i.e. positive) in the spectral interval 412–555 nm; (iv) the ratio of the standard deviation to the mean of satellite-derived $\tau_a(865)$ computed over the 5x5-pixel square is lower than 0.2; (v) the ratio of the standard deviation to the mean of *in situ* $\tau_a(870)$ computed over the measurements (collected in the ± 1 hour interval) is lower than 0.2. The latter criteria filter out conditions of strong spatial and/or temporal heterogeneity that would lessen the meaning of the comparison. Finally, the field value is computed as the average of the measurements in the ± 1 hour interval. The Ångström exponent ν is computed as the slope of the log-transformed data with respect to wavelength in the 443–870 nm interval.

The scatter plot of SeaWiFS-derived versus *in situ* aerosol optical thickness at 443, 500 and 865 nm for 59 match-ups is displayed in Fig. 10 (the satellite-derived $\tau_a(500)$ is simply computed as the mean of the output at 490 and 510 nm to match the centre-wavelength of the field instrument). This comparison is completed for the same match-ups by the scatter plot of SeaWiFS-derived versus *in situ* Ångström exponents (Fig. 11). The analysis gives satisfactory results for the aerosol optical thickness with an *RMSrd* between the two distributions of $\sim 25\%$ and a correlation coefficient r higher than 0.92 for the three wavelengths considered. The spectral agreement is supported by an *RMSrd* of 24% for the Ångström exponent. The range of values covered by the match-ups is 0.04–0.4 and 0.5–2.1 for $\tau_a(500)$ and ν, respectively: these values are very representative of the conditions encountered in the Baltic (see Section 2). The distribution of the Ångström exponent displays relatively high values, more typical of summer conditions on Gotland (half of the match-ups are actually from July and August).

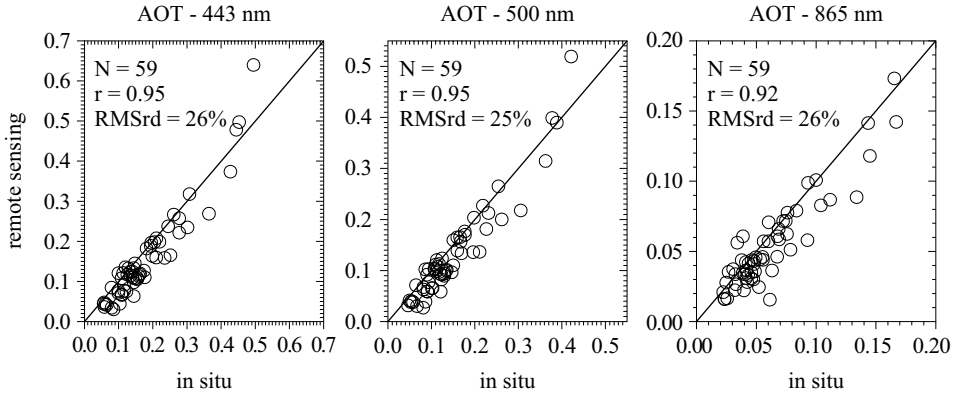

Fig. 10. Scatter plot of SeaWiFS-derived versus *in situ* aerosol optical thickness (AOT) at 443, 500, and 865 nm. N is the number of match-ups, r is the correlation coefficient and *RMSrd* the root mean square of relative differences

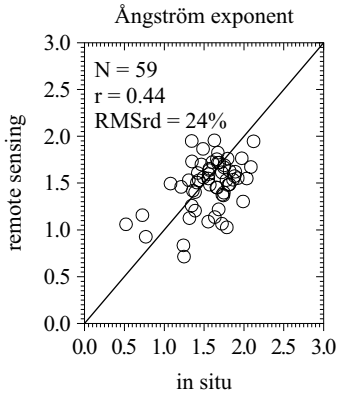

Fig. 11. Scatter plot of SeaWiFS-derived versus *in situ* aerosol Ångström exponent ν. N is the number of match-ups, r is the correlation coefficient and *RMSrd* the root mean square of relative differences

These results are in full agreement with those presented in Figs 2 and 3. As already stated, higher *RMSrd* values are naturally expected in the comparison of actual satellite retrievals and point field measurements. For instance, the sole introduction of noise sources at λ_7 and λ_8 can lead to substantial uncertainties in the estimated ν (Bulgarelli & Zibordi 2003).

4. Discussion and conclusions

The accurate interpretation of ocean colour data for the Baltic Sea is recognized as being a difficult task. The Baltic Sea is typically characterized by relatively high solar zenith angles (which increase atmospheric multiple

scattering), and high yellow substance absorption coefficients (which decrease the water signal, particularly in the blue part of the spectrum).

The accuracy analysis of an approximate atmospheric correction algorithm for the processing of SeaWiFS images, already investigated for atmospheric and water parameters typical of mid-latitude European regions, has been extended to the Baltic Sea.

The method accounts for Rayleigh multiple scattering, aerosol single scattering, Rayleigh-aerosol coupling, and accounts for a contribution of water-leaving radiances in the NIR channels. A vicarious calibration procedure is applied to trim model inaccuracies and space sensor absolute calibration uncertainties.

The highly accurate FEM radiative transfer code has been used to simulate the radiance distribution for representative atmosphere-water test cases. For all cases, the code accuracy has been assessed for the estimate of (i) aerosol optical thickness, (ii) water-leaving radiance, and (iii) remote sensing reflectance ratios.

When compared to mid-latitudes, the accuracy of the atmospheric correction method applied to Baltic Sea data remains almost unchanged for the estimation of the atmospheric parameters: the aerosol optical thickness at 865 nm and the aerosol Ångström exponent are determined with uncertainties lower than $\pm 5\%$ and $\pm 10\%$, respectively. These results are confirmed by the analysis of 59 match-ups between satellite derived and *in situ* measurements for a site located in the central Baltic. The latter comparison gives differences (expressed as *RMSrd*) of $\sim 25\%$ and a correlation higher than 0.92 for the aerosol optical thickness at 443, 500 and 865 nm.

Because of the relatively high yellow substance absorption, often combined with slanted solar illumination, the retrieval of the water-leaving radiance in the blue part of the spectrum is highly degraded, to the extent that almost no correlation is found between retrieved and simulated values. Better results are found at the other wavelengths.

The accuracy in the estimation of the remote sensing reflectance ratio R_{35} decreases with a decrease in chlorophyll a concentration and an increase in yellow substance absorption. The uncertainty ranges between $\pm 7\%$ for high chlorophyll a concentrations (i.e. 10 mg m^{-3}) and low yellow substance absorption (i.e. $a_{ys}(440) = 0.1443\ \mathrm{m}^{-1}$, $S_{ys} = 0.0193\ \mathrm{nm}^{-1}$), and $\pm 47\%$ for low chlorophyll a concentrations (i.e. 0.3 mg m^{-3}) and high yellow substance absorption (i.e. $a_{ys}(440) = 0.6831\ \mathrm{m}^{-1}$, $S_{ys} = 0.0193\ \mathrm{nm}^{-1}$). The propagation of the R_{35} uncertainty on Chl estimation, tested via the OC2v2 algorithm, shows values varying between $\pm 14\%$ for high chlorophyll a

concentrations and low yellow substance absorption, and ±200% for low chlorophyll a concentrations and high yellow substance absorption.

Keeping the same atmosphere-water conditions, it has been observed that the atmospheric correction scheme is quite sensitive to seasonal changes in the solar zenith, producing an overestimation of $\tau_a(\lambda_8)$, ν, $L_w(\lambda)$ and R_{35} during winter (i.e. for high θ_0), and their underestimation during summer (i.e. for low θ_0). The opposite occurs for Chl.

In the theoretical evaluation of the accuracy of the atmospheric correction method, a knowledge of the exact value of $L_w(\lambda_{7,8})$ and no instrumental noise in $L_{tot}(\lambda)$ were assumed. As already pointed out (Bulgarelli & Zibordi 2003), the introduction of noise at λ_7 and λ_8, accounting for the signal-to-noise ratio and the inexact prediction of the water-leaving radiance in the NIR, can lead to increased uncertainties in the estimated ν and $L_w(\lambda)$ at $\lambda_1 - \lambda_6$. This holds true mainly in the presence of heavy sediment loads. Other phenomena, like bottom reflection and the adjacency effect, can contribute to greater uncertainties, particularly in coastal areas. Bottom effects may lead to $L_w(\lambda_i)$ being overestimated at λ_5 and, to a lesser extent, at λ_4 and λ_3. The adjacency effect may produce spectral variations in the estimation of $L_w(\lambda_i)$ mainly as a function of the reflectance of the surrounding land cover. However, these uncertainties are strictly dependent on the features of each specific site and have thus been omitted from the present study. The results presented here support the following general conclusions on the atmospheric correction scheme:

(i) the accuracy of derived atmospheric products (i.e. the spectral aerosol optical thickness and the Ångström exponent) is relatively high, as confirmed by the analysis of match-ups between satellite-derived and *in situ* measurements;

(ii) the determination of the water-leaving radiance fails in the blue part of the spectrum, but shows different levels of accuracy at the other wavelengths as a function of the atmospheric and marine constituents. It is worth stressing that misestimation of the water-leaving radiance in the blue part of the spectrum also occurs in other widely used processing codes (Zibordi et al. 2003);

(iii) the estimation of the remote sensing reflectance ratio at λ_3 and λ_5 (used in many bio-optical algorithms) exhibits an accuracy that could be acceptable for environmental studies (exceptions are the cases characterized by low pigment concentrations associated with high yellow substance absorption).

The evaluation of the accuracy of satellite-derived data using match-ups of *in situ* and SeaWiFS data was only performed for atmospheric

parameters, but a proper validation of the satellite-derived marine parameters on the basis of highly accurate *in situ* measurements is obviously also desirable. Lastly, the general results of the present paper once more underline the urgent need for more advanced algorithms for the interpretation of optical remote sensing marine data, leading to a better integration of the atmosphere and water systems.

Acknowledgements

Professor B. Håkansson is duly acknowledged for providing the AERONET *in situ* aerosol optical thickness data from Gotland Island.

The authors would like to thank the SeaWiFS Project (Code 970.2) and the Distributed Active Archive Center (Code 902) at the Goddard Space Flight Center for the production and the distribution of these data, respectively.

References

Bulgarelli B., Mélin F., 2000, *SeaWiFS data processing code REMBRANDT version 1.0*, Rep. EUR 19514 EN.

Bulgarelli B., Kisselev V., Roberti L., 1999, *Radiative transfer in the atmosphere-ocean system: the finite element method*, Appl. Opt., 38, 1530–1542.

Bulgarelli B., Zibordi G., 2003, *Remote sensing of ocean colour: accuracy assessment of an approximate atmospheric correction method*, Int. J. Remote Sens., 24, 491–509.

Darecki M., Weeks A., Sagan S., Kowalczuk P., Kaczmarek S., 2003, *Optical characteristics of two contrasting case 2 waters and their influence on remote sensing algorithms*, Cont. Shelf Res., 23, 237–250.

Ferrari G. M., Dowell M. D., Grossi S., Targa C., 1996, *Relationship between the optical properties of chromophoric dissolved organic matter and total concentration of dissolved organic carbon in the southern Baltic Sea region*, Mar. Chem., 55, 299–316.

Højerslev N. K., Aas E., 2001, *Spectral light absorption by yellow substance in the Kattegat-Skagerrak area*, Oceanologia, 43 (1), 39–60.

Holben B. N., Eck T. F., Slutsker I., Tanré D., Buis J. P., Setzer A., Vermote E., Reagan J. A., Kaufman Y. J., Nakajima T., Lavenu F., Jankowiak I., Smirnov A., 1998, *AERONET – a federated instrument network and data archive for aerosol characterization*, Remote Sens. Environ., 66, 1–16.

Hooker S. B., Esaias W. E., 1993, *An overview of the SeaWiFS project*, EOS Trans. Amer. Geophys. Union, 74, 241–246.

International Association for Meteorology and Atmospheric Physics. Radiation Commission (IAMPRC), 1984, *A preliminary cloudless standard atmosphere for radiation computation*, WCP-112, WMO/TD-No. 24, Boulder.

Kononen K., Leppänen J.-M., 1997, *Patchiness, scales and controlling mechanisms of cyanobacterial blooms in the Baltic Sea: Application of a multi-scale research strategy*, [in:] *Monitoring algal blooms*, M. Kahru & C. W. Brown (eds.), Springer-Verl., Berlin, 63–84.

Kowalczuk P., 1999, *Seasonal variability of yellow substance absorption in the surface layer of the Baltic Sea*, J. Geophys. Res., 104, 30047–30058.

Kowalczuk P., Darecki M., 1998, *The relative share of light absorption by yellow substances in total light absorption in the surface layer of southern Baltic Sea*, paper 1052, pp. 9, S. G. Ackleson (ed.), Proc. 14th Conf. Ocean Optics, 10–13 November 1998, Kailua-Kona (Hawaii).

Kuśmierczyk-Michulec J., Marks R., 2000, *The influence of sea-salt aerosols on the atmospheric extinction over the Baltic and the North Seas*, J. Aerosol Sci., 31, 1299–1316.

Kuśmierczyk-Michulec J., Schulz M., Ruellan S., Krüger O., Plate E., Marks R., de Leeuw G., Cachier H., 2001, *Aerosol composition and related optical properties in the marine boundary layer over the Baltic Sea*, J. Aerosol Sci., 32, 933–955.

Larsson U., Elmgren R., Wulff F., 1985, *Eutrophication and the Baltic Sea: Causes and consequences*, Ambio, 14, 10–14.

Larsson U., Hajdu S., Walve J., Elmgren R., 2001, *Baltic Sea nitrogen fixation estimated from the summer increase in upper mixed layer total nitrogen*, Limnol. Oceanogr., 46, 811–820.

Maritorena S., O'Reilly J. E., 2000, OC2v2: *Update on the initial operational SeaWiFS chlorophyll a algorithm* NASA Tech. Memo. 2000–206892, Vol. 11, pp. 3–8, S. B. Hooker & E. R. Firestone (eds.), NASA Goddard Space Flight Center, Greenbelt, Maryland.

Mélin F., Steinich C., Gobron N., Pinty B., Verstraete M. M., 2002, *Optimal merging of LAC and GAC data from SeaWiFS*, Int. J. Remote Sens., 23, 801–807.

Mélin F., Zibordi G., Berthon J.-F., 2003, *Assessment of SeaWiFS atmospheric and marine products for the Northern Adriatic Sea*, IEEE Trans. Geosci. Remote Sens., 41, 548–558.

Neumann T., Fennel W., Kemp C., 2002, *Experimental simulations with an ecosystem model of the Baltic Sea: A nutrient load reduction experiment*, Global Biogeochem. Cycles, 16, 10.1029/2001GB001450.

Ohde T., Sturm B., Siegel H., 2002, *Derivation of SeaWiFS vicarious calibration coefficients using in situ measurements in Case 2 water of the Baltic Sea*, Remote Sens. Environ., 80, 248–255.

Olszewski J., Sagan S., Darecki M., 1992, *Spatial and temporal changes in some optical parameters in the southern Baltic*, Oceanologia, 33, 87–102.

Schwarz J. N., Kowalczuk P., Kaczmarek S., Costa G. F., Mitchell B. G., Kahru M., Chavez F. P., Cunningham A., McKee D., Gege P., Kishino M., Phinney D. A., Raine R., 2002, *Two models for absorption by coloured dissolved organic matter (CDOM)*, Oceanologia, 44 (2), 209–241.

Siegel H., Gerth M., 1999, *Remote sensing studies of the exceptional summer of 1997 in the Baltic Sea: The warmest August of the century, the Oder flood, and phytoplankton blooms*, [in:] *Satellites, oceanography and society*, D. Halpern (ed.), Elsevier, Amsterdam, 239–255.

Siegel H., Gerth M., Neumann T., Doerffer R., 1999, *Case studies on phytoplankton blooms in coastal and open waters of the Baltic Sea using Coastal Zone Color Scanner data*, Int. J. Remote Sens., 20, 1249–1264.

Smirnov A., Holben B. N., Kaufman Y. J., Dubovik O., Eck T. F., Slutsker I., Pietras C., Halthore R. N., 2002, *Optical properties of atmospheric aerosols in marine environments*, J. Atmos. Sci., 59, 501–523.

Sturm B., Zibordi G., 2002, *SeaWiFS atmospheric correction by an approximate model and vicarious calibration*, Int. J. Remote Sens., 23, 489–501.

Witek Z., Ochocki S., Maciejowska M., Pastuszak M., Nakonieczny J., Podgórska B., Kownacka J. M., Mackiewicz T., Wrzesińska-Kwiecień, 1997, *Phytoplankton primary production and its utilization by the pelagic community in the coastal zone of the Gulf of Gdańsk (southern Baltic)*, Mar. Ecol. Prog. Ser., 148, 169–186.

Zernova V. V., 1997, *Autumn Baltic phytoplankton*, Oceanology, 37, 215–222.

Zibordi G., Berthon J. F., Doyle J. P., Grossi S., van der D. Linde, Targa C., Alberotanza L., 2002, *Coastal Atmosphere and Sea Time Series (CoASTS), Part 1: A long-term measurement program*, NASA Tech. Memo. 2002–206892, Vol. 19, pp. 1–29, S. B. Hooker & E. Firestone (eds.), NASA Goddard Space Flight Center, Greenbelt, Maryland.

Zibordi G., Mélin F., Hooker S. B., D'Alimonte D., Holben B., 2003, *An Autonomous Above-Water System for the Validation of Ocean Color Radiance Data*, IEEE Trans. Geosci. Remote Sens.